# Computational design of a red fluorophore ligase for site-specific protein labeling in living cells

Daniel S. Liu[a], Lucas G. Nivón[b], Florian Richter[b,c,1], Peter J. Goldman[a], Thomas J. Deerinck[d], Jennifer Z. Yao[a], Douglas Richardson[e], William S. Phipps[a], Anne Z. Ye[a], Mark H. Ellisman[d,f], Catherine L. Drennan[a,g,h], David Baker[b,i], and Alice Y. Ting[a,2]

Departments of [a]Chemistry and [g]Biology and [h]Howard Hughes Medical Institute, Massachusetts Institute of Technology, Cambridge, MA 02139; [b]Department of Biochemistry, [i]Howard Hughes Medical Institute, and [c]Graduate Program in Biological Physics, Structure and Design, University of Washington, Seattle, WA 98195; [d]National Center for Microscopy and Imaging Research, Center for Research on Biological Systems and [f]Department of Neurosciences, University of California, San Diego, La Jolla, CA 92093; and [e]Department of NanoBiophotonics, Max Planck Institute for Biophysical Chemistry, 37077 Göttingen, Germany

Edited by Xiaowei Zhuang, Harvard University and Howard Hughes Medical Institute, Cambridge, MA, and approved August 25, 2014 (received for review March 12, 2014)

**Chemical fluorophores offer tremendous size and photophysical advantages over fluorescent proteins but are much more challenging to target to specific cellular proteins. Here, we used Rosetta-based computation to design a fluorophore ligase that accepts the red dye resorufin, starting from *Escherichia coli* lipoic acid ligase. X-ray crystallography showed that the design closely matched the experimental structure. Resorufin ligase catalyzed the site-specific and covalent attachment of resorufin to various cellular proteins genetically fused to a 13-aa recognition peptide in multiple mammalian cell lines and in primary cultured neurons. We used resorufin ligase to perform superresolution imaging of the intermediate filament protein vimentin by stimulated emission depletion and electron microscopies. This work illustrates the power of Rosetta for major redesign of enzyme specificity and introduces a tool for minimally invasive, highly specific imaging of cellular proteins by both conventional and superresolution microscopies.**

fluorescence microscopy | enzyme redesign | LplA | PRIME | chemical probe targeting

Fluorescent proteins are used ubiquitously in imaging, but their dim fluorescence, rapid photobleaching, and large size limit their utility. At ~27 kDa (~240 aa), fluorescent proteins can disrupt protein folding and trafficking or impair protein function (1, 2). Chemical fluorophores, in comparison, are typically less than 1 kDa in size, and are brighter and more photostable. These properties allow chemical fluorophores to perform better than fluorescent proteins in advanced imaging modalities such as single-molecule tracking and superresolution microscopies (3, 4).

Site-specific labeling of proteins with chemical fluorophores inside living cells is challenging because these fluorophores are not genetically encodable and therefore must be posttranslationally targeted inside a complex cellular milieu. Existing methods to achieve this targeting either require large fusion tags [such as HaloTag (5), the SNAP tag (6), and the DHFR tag (7)] or have insufficient specificity [such as biarsenical dye targeting (8) and amber codon suppression (9)]. To achieve a labeling specificity comparable to fluorescent proteins, we developed PRIME (PRobe Incorporation Mediated by Enzymes), which uses *Escherichia coli* lipoic acid ligase to attach small molecules to a 13-aa peptide tag (Fig. 1*A*) (10). To make PRIME more useful for cellular protein imaging, we sought to engineer the system for the targeting of bright chemical fluorophores. The challenge, though, is that lipoic acid ligase (LplA) has a small and fully enclosed substrate-binding pocket that even with extensive structure-guided mutagenesis has not until this point been able to accommodate large chemical structures.

## Results

**Synthesis of Resorufin Derivatives for PRIME.** We considered fluorophores for PRIME based on the steric constraints of LplA. Far-red emitters such as Cy5 and Atto 647N, although photophysically desirable, are so bulky that binding inside LplA would require major reconstruction of protein backbone. Boron-dipyrromethenes (BODIPYs) are small fluorophores with tunable emission but their hydrophobicity causes nonspecific binding to cells. In comparison, the small red phenoxazine fluorophore resorufin does not bind to intracellular structures. It spectrally overlaps with the commonly used fluorescent protein mCherry, but resorufin is twice as bright, comparable to Cy3 (brightness is defined as extinction coefficient multiplied by fluorescence quantum yield). In addition to its conventional fluorescence readout, resorufin can also be used for single-molecule imaging (11), chromophore-assisted light inactivation (12), and contrast generation for EM by photoxidation (13). Compared with miniSOG, a genetically encoded dual fluorescence/EM tag, resorufin is red-shifted in emission, approximately nine times brighter, yet ~40 times smaller (by mass) (14). Resorufin therefore has suitable photophysical attributes for PRIME.

To develop a resorufin ligase, we first synthesized two variants with carboxylic acid functionalities and different linker lengths (Fig. 1*B*), for binding and activation by LplA as adenylate esters. To incorporate this tricyclic structure into the enzyme binding pocket, which only has room for the five-membered ring dithiolane of lipoic acid, is a formidable challenge. Even if mutagenesis

### Significance

This work establishes a fluorescence labeling method that can be used in living cells to derivatize specific proteins of interest with a small red fluorophore, resorufin. The method has extremely high sequence specificity and is based on a computationally designed fluorophore ligase, derived from *Escherichia coli* lipoic acid ligase. These results demonstrate the power of computational design to majorly reengineer enzyme specificity. Extensive screening of rationally designed enzyme mutants failed to achieve the same result.

Author contributions: D.S.L., L.G.N., F.R., P.J.G., C.L.D., D.B., and A.Y.T. designed research; D.S.L., L.G.N., F.R., P.J.G., T.J.D., J.Z.Y., D.R., W.S.P., and A.Z.Y. performed research; D.S.L., L.G.N., F.R., P.J.G., J.Z.Y., D.R., W.S.P., and A.Z.Y. contributed new reagents/analytic tools; D.S.L., L.G.N., F.R., P.J.G., T.J.D., D.R., M.H.E., C.L.D., and A.Y.T. analyzed data; and D.S.L., L.G.N., and A.Y.T. wrote the paper.

Conflict of interest statement: A patent application for lipoic acid ligase-based protein labeling technology has been filed by Massachusetts Institute of Technology.

This article is a PNAS Direct Submission.

Freely available online through the PNAS open access option.

Data deposition: Crystallography, atomic coordinates, and structure factors have been deposited in the Protein Data Bank, www.pdb.org (PDB ID codes 4TVW and 4TVY).

[1]Present address: Institute of Biology, Humboldt-Universität zu Berlin, 10099 Berlin, Germany.

[2]To whom correspondence should be addressed. Email: ating@mit.edu.

This article contains supporting information online at www.pnas.org/lookup/suppl/doi:10.1073/pnas.1404736111/-/DCSupplemental.

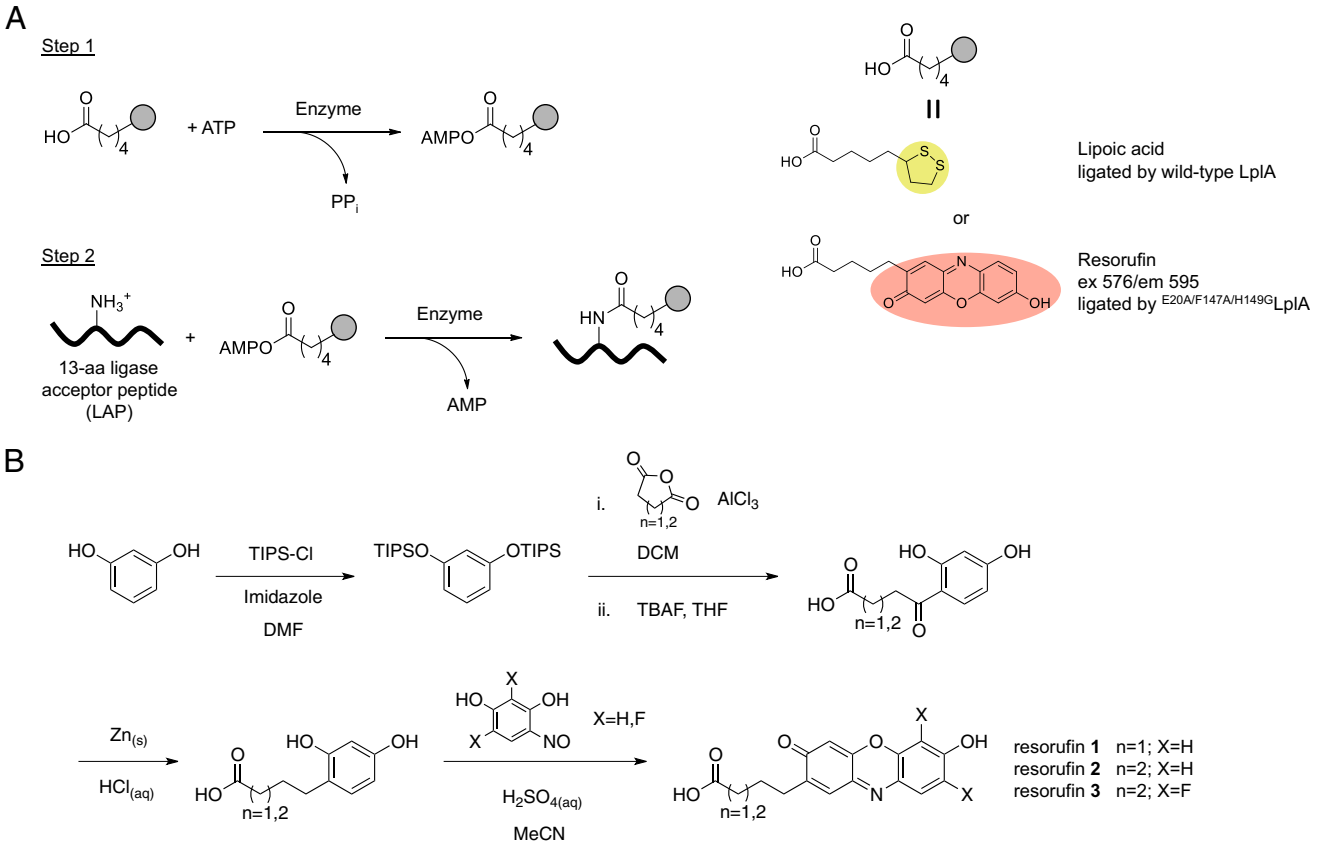


**Fig. 1.** Enzyme-catalyzed site-specific ligation of a resorufin fluorophore to a peptide. (*A*) (*Left*) In PRIME labeling, an enzyme catalyzes the covalent ligation of a small molecule probe onto the lysine residue of a 13-aa recognition peptide (LAP) in two steps. First, the probe is activated as an AMP ester; second, the activated probe is transferred onto LAP. (*Right*) Natural and unnatural substrates of LplA. Wild-type LplA ligates lipoic acid. In this work, we computationally designed a triple mutant $^{E20A/F147A/H149G}$LplA to ligate the red fluorophore resorufin. (*B*) Syntheses of three potential resorufin substrates for LplA. Resorufin **3** is a difluorinated isostere of resorufin **2**. DCM, dichloromethane; DMF, *N*,*N*-dimethylformamide; MeCN, acetonitrile; TBAF, tetra-*n*-butylammonium fluoride; THF, tetrahydrofuran; TIPS-Cl, triisopropylsilyl chloride.

could create such a space, it is not clear whether such drastic changes in the core of the enzyme would be detrimental to LplA folding and catalysis.

**Structure-Based Mutagenesis and Screening for Resorufin Ligase Activity.** We could not detect any resorufin ligation activity using the wild-type enzyme under forcing conditions (discussed below). All previous LplA mutants that recognize an unnatural substrate contain a mutation at Trp37, which we call a "gatekeeper" (Fig. 2*A*). A Trp37→Val mutation, for example, allows binding to a small blue coumarin fluorophore (10). Additionally, the Glu20 side chain also sterically limits the substrate binding pocket and may electrostatically repel negatively charged substrates (15), such as resorufin. Therefore, we screened the resorufin probes **1** and **2** against a library of nineteen Trp37 single and Glu20/Trp37 double mutants, in an attempt to detect resorufin ligation activity. Ligation of resorufin **2** was detected with three LplA mutants, with the single mutant $^{W37V}$LplA performing the best (*SI Appendix*, Fig. S1*A*), but the ligation efficiencies (less than 20% conversion in 4 h with 2 μM enzyme) were far too low to be useful. Crude modeling shows that the Trp37→Val mutation may sufficiently lengthen the substrate binding tunnel for resorufin **2** as it does for coumarin, but ring 1 of resorufin **2** clashes with the Arg70 sidechain, which is structurally important for LplA's substrate binding loop (*SI Appendix*, Fig. S1*B*). This steric clash is worse for the shorter resorufin **1** because its ring 1 is brought closer to the Arg70 sidechain, which may explain the complete lack of activity in our screen (*SI Appendix*, Fig. S1*A*).

**Rosetta Computational Design of a Resorufin Ligase.** Although these results with gatekeeper mutagenesis were disappointing, we imagined that the fully aliphatic linker of our resorufin **2** substrate might provide sufficient flexibility for it to bind in previously unimagined ways. A high-quality crystal structure of wild-type LplA in complex with lipoyl-AMP is available (16) and permitted us to explore the use of Rosetta (17) to computationally expand our search space for a resorufin ligase. In previous work, computation was used to alter the specificity of a deaminase enzyme for ammelide (a one-ring structure) instead of guanine (two rings) (18), a DNA endonuclease for altered sequence recognition (19), and an amino acid adenylation domain for leucine instead of phenylalanine (20). Our problem of engineering LplA to ligate resorufin instead of lipoic acid presents a significantly greater challenge owing to the large size and shape difference between the original and new substrates.

For our design efforts we chose to work with resorufin **2** (referred to below as "resorufin") because it alone exhibited detectable activity in our rationally designed mutant screens. Our design strategy was to mutate residues at the lipoyl binding pocket while avoiding mutations near the phosphocarboxylic anhydride bond known to be important for catalysis. We sought to use Rosetta to accommodate resorufin-AMP instead of resorufin plus ATP because the binding order of the latter two is not known, and it is likely that binding of either causes a conformational change in the enzyme (16). We used a fixed-backbone Rosetta design procedure as follows (17). First, a library of low-energy resorufin-AMP rotamers was prepared, in which the resorufin moiety was allowed

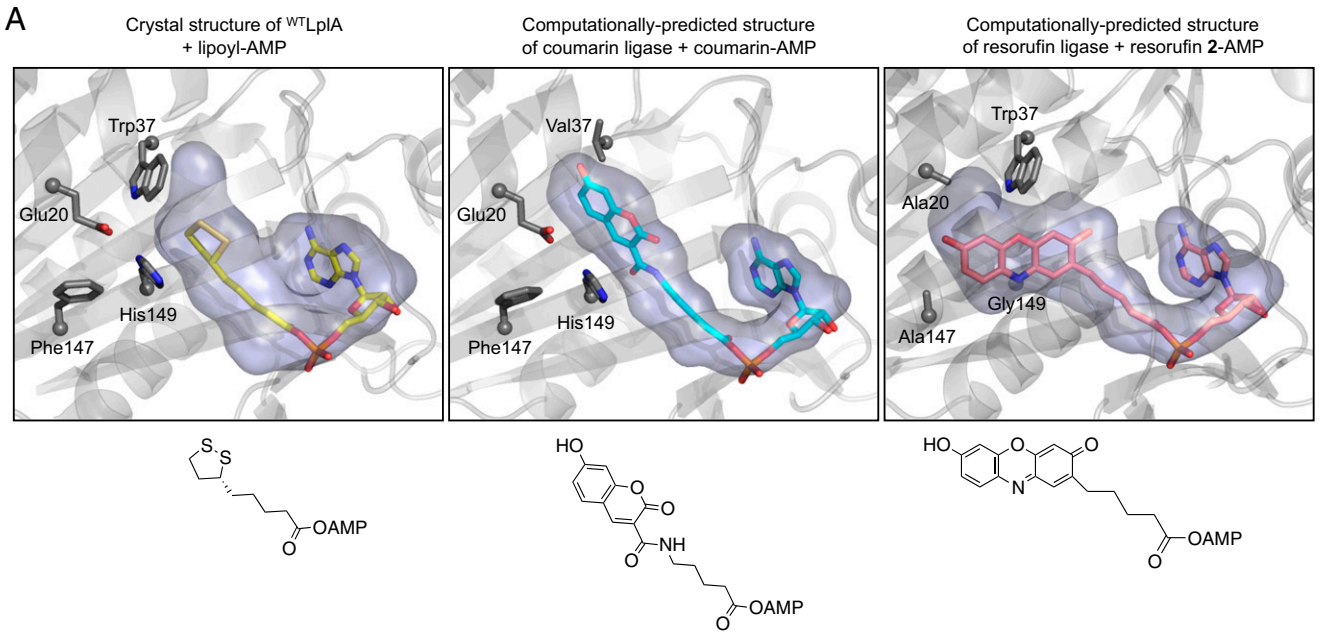


B

| Ligase mutant | % Yield |
|---|---|
| E20A / F147A / H149G (resorufin ligase) | 100 |
| E20A / F147A | 40 |
| E20A / F147G | 5 |
| F147A / H149G | N.D. |
| F147A | N.D. |
| H149G | N.D. |
| E20A | N.D. |
| W37V (coumarin ligase) | N.D. |

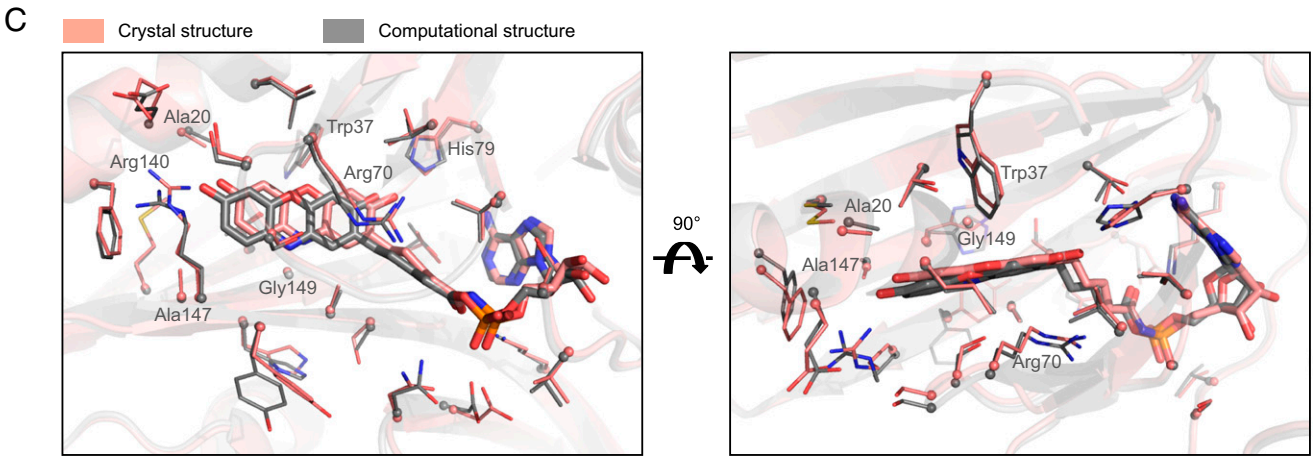


**Fig. 2.** Computational design of a resorufin fluorophore ligase and design analysis by X-ray crystallography. (*A*) Cut-away views of wild-type LplA, coumarin ligase, and resorufin ligase in complex with their AMP ester intermediates. Substrate adenylate esters and key substrate binding pocket residues are rendered in sticks. $C_\alpha$ of labeled residues are shown as gray balls. (*Left*) Panel from a crystal structure (PDB ID code 3A7R) (16). In coumarin ligase (*Middle*), the "gatekeeper" Trp37 is mutated to Val37 to accommodate the coumarin fluorophore. In the designed resorufin ligase (*Right*), Trp37 is left intact but Glu20→Ala, Phe147→Ala, and His149→Gly mutations are introduced to accommodate the resorufin fluorophore. The inner surfaces of the substrate binding pockets were generated using Hollow software (47) and are shown in light blue. The chemical structures of lipoyl-AMP, coumarin-AMP, and resorufin-AMP are shown below each panel in their approximate binding conformations. (*B*) Activity of resorufin ligase and other LplA with constituent mutations for the ligation of 500 μM resorufin **2** to LAP peptide in 90 min with 2 μM enzyme. (*C*) The crystal structure of resorufin ligase with a nonhydrolyzable substrate analog, resorufin sulfamoyladenosine, was obtained by X-ray diffraction at 3.5-Å resolution. The substrate binding pocket of the crystal structure (salmon) is shown here overlaid with the computational structure (gray, from the top-ranked triple mutant design conformer 7_33) in a cut-away view at two different angles. Resorufin substrates are shown in thick sticks; ligase residues within 4 Å of the resorufin moiety are shown in thin sticks. The chemical structure of resorufin sulfamoyladenosine and a close-up view of the binding pocket are shown in *SI Appendix*, Fig. S4 *B–D*.

to move, whereas AMP was held constant in the conformation observed in the LplA·lipoyl-AMP crystal structure. Second, the resorufin-AMP rotamer library was superimposed onto the AMP position in the LplA crystal structure with wild-type sequence to create the starting model for Rosetta calculations. Third, LplA residues within 6–8 Å of the resorufin moiety were automatically selected, yielding roughly 24 designable residues (with the exact number depending on the conformer of resorufin at each given point during the simulation), resulting in a theoretical sequence space of $20^{24}$. This set included mutations at the gatekeeper Trp37 and Glu20. Residues near AMP were fixed in identity and rotameric state throughout the calculations to preserve the favorable AMP binding energy. Fourth, 1,600 independent runs of the Rosetta algorithm were implemented, using Monte Carlo sampling to implicitly explore $\sim 10^6$ sequences in each run. Thus, $\sim 10^9$ out of the $20^{24}$ possible sequences were calculated. The resulting 1,600 energy-minimized computational designs converged on nine unique LplA sequences. These were filtered by overall Rosetta score and other criteria of structure quality, then ranked according to resorufin-AMP binding energy (*SI Appendix*, Fig. S2). Strikingly, 190 out of the top 216 designs had an identical sequence: the triple mutant E20A/F147A/H149G of LplA.

It was surprising to us that this triple mutant contains no mutation at the gatekeeper residue Trp37. Instead, Rosetta converged on a design that placed the resorufin binding pocket in a different and unexpected location (Fig. 2*A*), bent ∼45° with respect to the predicted binding pocket for coumarin in $^{W37V}$LplA. Resorufin-AMP twists at the benzylic carbon to enter the cavity carved out by removal of bulky side chains at residues 20, 147, and 149.

**In Vitro Activity of Resorufin Ligase.** In an HPLC assay, this triple mutant ($^{E20A/F147A/H149G}$LplA) catalyzed the ligation of resorufin to the 13-aa ligase acceptor peptide (LAP) in an ATP-dependent manner, and the product was confirmed by mass spectrometry (*SI Appendix*, Fig. S3 *A* and *B*). We scanned the excitation and emission profiles of the peptide-resorufin adduct and found that ligation did not shift these wavelengths (*SI Appendix*, Fig. S3*C*). Although 2 μM enzyme gave 100% conversion to product in 90 min (Fig. 2*B*), under matched conditions the constituent single mutations and the rationally designed W37V mutant exhibited no detectable activity, whereas the double mutants E20A/F147A and F147A/H149G exhibited greatly reduced activity (Fig. 2*B*). Quantitative analysis of this triple mutant, which we call "resorufin ligase," gave a $k_{cat}$ of 3.4 $min^{-1}$ and a $K_M$ of 35 μM for resorufin (*SI Appendix*, Fig. S3 *D* and *E*). This represents an enormous catalytic enhancement compared to wild-type LplA, whose ligation of resorufin is below our detection limit. Overall the catalytic efficiency of resorufin ligase is 81-fold worse than the wild-type enzyme for lipoic acid ligation (21) but fivefold better than our best previous fluorophore ligase [coumarin ligase (10)], which was designed rationally.

**Resorufin Ligase Crystal Structure.** To determine whether the actual structure of resorufin ligase matched that of the computational design, we cocrystallized resorufin ligase in the presence of resorufin and ATP to generate resorufin-AMP in situ. In the absence of a protein substrate, we expected resorufin ligase to retain resorufin-AMP, as the wild-type ligase does with lipoyl-AMP (16). It was important to obtain a substrate-adenylate ester-bound crystal structure because binding induces a large conformational change in the enzyme's active site (16), such that the Rosetta-designed binding pocket would not be formed in the apo ligase. We found, however, that crystals formed this way did not harbor electron density for resorufin-AMP in the expected binding site, and the 2.2 Å-resolution structure possessed tertiary features matching the apo form of wild-type LplA (22) (*SI Appendix*, Fig. S4*A*). Because separate experiments showed that these crystals were capable of forming resorufin-AMP, we postulated that this high-energy intermediate dissociated from the active site and hydrolyzed over the 3-d crystallization period.

We therefore synthesized a nonhydrolyzable substrate analog, resorufin sulfamoyladenosine (structure in *SI Appendix*, Fig. S4*B*), for cocrystallization. Sulfamoyladenosine analogs have been used to generate competitive inhibitors of aminoacyl-tRNA synthetases (23), and biotin sulfamoyladenosine is a competitive inhibitor of *E. coli* biotin ligase (24), an enzyme structurally and functionally homologous to LplA (25, 26). We confirmed that resorufin ligase was able to bind resorufin sulfamoyladenosine and proceeded to crystallize the ligase in the presence of this analog. The resulting crystals exhibited a different space group and produced a 3.5-Å resolution structure after correction for diffraction anisotropy (data processing in *SI Appendix*, *Supporting Methods* and Table S1). We observed clear electron density for the resorufin substrate (*SI Appendix*, Fig. S4*C*) and found that the crystal structure closely matched the computational design (Fig. 2*C*). Resorufin points toward residues 20 and 147, although an ∼1-Å translation of the resorufin core relative to the design potentially allows it to form two hydrogen bonds, with Arg140 and His79 sidechains, instead of the one hydrogen bond predicted by Rosetta (*SI Appendix*, Fig. S4*C*). Arg70 does not clash with the ring 1 of resorufin but instead forms a favorable stacking interaction (Fig. 2*C*). Comparing the apo and substrate-bound structures, we further observed that resorufin ligase undergoes the same global conformational change as wild-type LplA does upon substrate binding, including the clamping down of two substrate binding loops and a ∼180° rotation of the C-terminal domain (*SI Appendix*, Fig. S4*A*). It was interesting to us that the major cavity carving by Rosetta did not impede these essential dynamic features of the enzyme.

**Protein Labeling in Living Cells with Resorufin Ligase.** We proceeded to test resorufin labeling inside cells. First it was necessary to mask the acidic groups on resorufin as an acetoxymethyl (AM) ester and ether to give resorufin-$AM_2$. This probe readily crossed cell membranes; endogenous esterases then cleave the masking groups to regenerate resorufin (27). We observed that resorufin-$AM_2$ has two regioisomers, *cis* and *trans* (*SI Appendix*, Fig. S5*A*). When we separately tested the retention of the two isomers in untransfected cells, we found that the *trans* isomer exhibited less nonspecific binding, leading to lower fluorescence background after washout (*SI Appendix*, Fig. S5*B*), even though both isomers entered cells equally well, and their unmasked products are identical. It is possible that the *cis* isomer associates more strongly with intracellular membranes or is a poorer substrate for endogenous esterases. We therefore performed all subsequent experiments with pure *trans* resorufin-$AM_2$. For cellular experiments we relied on intracellular ATP to effect ligation and endogenous organic anion transporters to remove excess unconjugated dye during the washout step following protein labeling (10).

To characterize labeling specificity we transfected human embryonic kidney 293T (HEK) cells with GFP-tagged resorufin ligase and LAP-tagged blue fluorescent protein (BFP), then treated these cells with resorufin-$AM_2$ for 10 min. After a further 45-min dye washout step we imaged these cells live and observed labeling only in cells expressing both ligase and LAP, and not in neighboring cells lacking either or both constructs (Fig. 3*A*). Resorufin retention was also not observed in negative controls where LAP-BFP was replaced by a point mutant (LAP Lys→Ala), or where resorufin ligase was replaced by wild-type LplA.

We analyzed the lysates of resorufin-labeled cells by SDS/PAGE and observed a single red fluorescent band at the molecular weight of LAP-BFP (Fig. 3*B*). Using a gel-shift assay on cell lysates, we determined that the labeling yield reached 74% in HEK cells treated with 5 μM resorufin-$AM_2$ for 30 min (*SI Appendix*, Fig. S6).

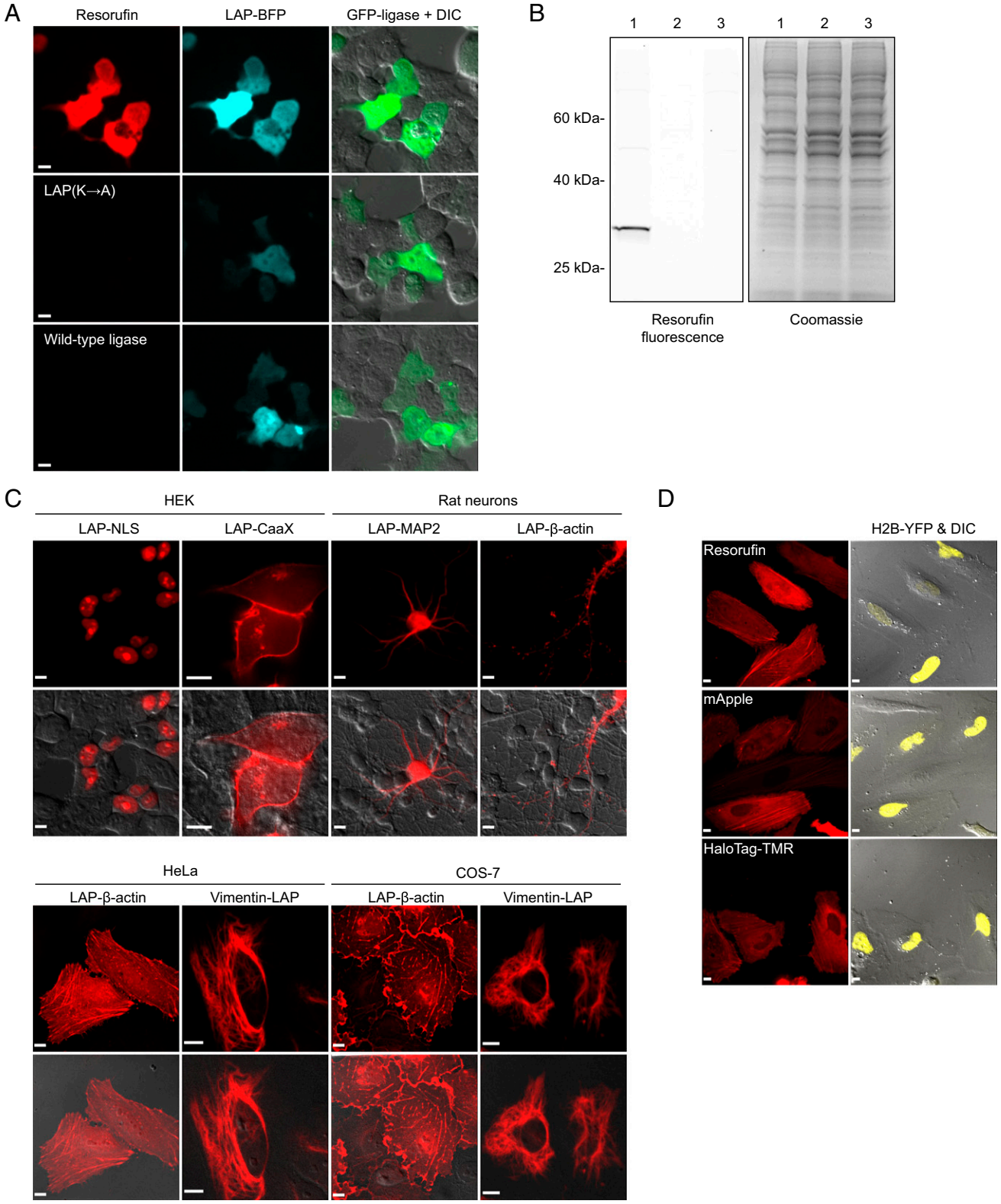


**Fig. 3.** Site-specific protein labeling with resorufin ligase in living mammalian cells. (*A*) Human embryonic kidney 293T (HEK) cells coexpressing GFP-tagged resorufin ligase and LAP-BFP were labeled with 5 μM resorufin-$AM_2$ for 10 min, then washed for 45 min before live-cell imaging. Negative controls are shown with an alanine mutation in LAP and resorufin ligase replaced by wild-type LplA. (*B*) Gel analysis of labeling specificity. Cells labeled live as in *A* were lysed, resolved by SDS/PAGE, and visualized by fluorescence (*Left*) and Coomassie stain (*Right*). Negative controls using wild-type LplA (lane 2) or a Lys→Ala mutation in LAP (lane 3) showed diminished signal. (*C*) Resorufin labeling of various LAP fusion constructs in multiple mammalian cell lines (HEK, HeLa, and COS-7) and rat cortical neurons. Resorufin fluorescence is overlaid with differential interference contrast image in the lower panels. Labeling specificity of LAP–β-actin and vimentin-LAP compared with immunofluorescence is shown in *SI Appendix*, Fig. S7. CaaX, prenylation motif; NLS, nuclear localization signal. (*D*) Comparison of β-actin labeling in living HeLa cells by resorufin ligase versus mApple and HaloTag (using tetramethylrhodamine HaloTag ligand). In the latter two cases, actin is frequently excluded from the nucleus. H2B-YFP is a cotransfected nuclear marker. (All scale bars, 10 μm.)

Resorufin ligase could specifically label proteins localized to the nucleus and to the inner leaflet of the plasma membrane as well as β-actin, the intermediate filament protein vimentin, and microtubule-associated protein MAP2 with high sensitivity and specificity inside HeLa, COS-7, and cultured rat neurons (Fig. 3*C* and *SI Appendix*, Fig. S7). Labeling of β-actin in particular illustrates the benefits of a small, 2-kDa tag, because analogous mApple-β-actin (27-kDa tag size) and HaloTag-β-actin (35-kDa tag size) constructs displayed aberrant localization (Fig. 3*D*). Previous studies have also shown that fluorescent protein-tagged β-actin has impaired dynamics and altered affinity for actin binding proteins (28).

For extracellular labeling of surface proteins we found it advantageous to use the fluorinated resorufin **3** probe (Fig. 1*B*), whose reduced phenolic $pK_a$ compared with resorufin **2** confers two advantages. First, resorufin **3** is predominantly anionic and fluorescent at physiological pH (SI Appendix, Fig. S8*B*), so it does not leak into cells like resorufin **2** does when supplied at high concentrations, allowing users to bypass the lengthy washout step to remove the intracellular fluorophore pool (*SI Appendix*, Fig. S8*C*). Second, resorufin **3** remains bright at reduced pH values, allowing continued visualization of surface proteins after endocytosis into acidic compartments (*SI Appendix*, Fig. S8*C*).

Even though the resorufin excitation and emission wavelengths do not change significantly upon ligation to LAP (*SI Appendix*, Fig. S3*C*), we observed a fourfold reduction in fluorescence intensity, which may be due to photoinduced electron transfer to the +2 Trp of LAP (29). Mutation of this residue to Phe, to give LAP-F, reduced the intensity drop to ∼1.5-fold (*SI Appendix*, Fig. S9*B*), but the ligation efficiency declined by 1.8-fold in a single-time-point assay. We therefore recommend the standard LAP for most applications and LAP-F for experiments such as single-molecule imaging where fluorophore brightness is crucial.

Using the standard LAP sequence and a 30-min labeling protocol we observed a greater than 2:1 signal-to-noise ratio in imaging with as little as ∼0.8 μM of intracellular LAP target (*SI Appendix*, Fig. S10). This is similar to the ∼0.5 μM sensitivity limit of mCherry tagging measured in the same way (*SI Appendix*, *Supporting Methods*) (30). The reduction of resorufin fluorescence intensity upon ligation, therefore, does not significantly hinder labeling sensitivity compared with fluorescent protein tagging.

**Orthogonal Fluorophore Recognition by Resorufin and Coumarin Ligases.** Because resorufin and coumarin ligases bind their fluorescent substrates in distinct binding pockets, we tested whether recognition by these ligases could be orthogonal. We found that purified coumarin ligase does not ligate resorufin to LAP and purified resorufin ligase does not ligate coumarin, even though coumarin is smaller than resorufin (*SI Appendix*, Fig. S11 *A* and *B*). This orthogonality enabled us to simultaneously perform resorufin and coumarin labeling of resorufin ligase-expressing live cells mixed with coumarin ligase-expressing live cells (*SI Appendix*, Fig. S11*C*). Resorufin was observed to selectively partition to the former and coumarin selectively to the latter.

For fully orthogonal two-color labeling of different proteins within the same cell, rather than separate neighboring cells as shown here, it will be necessary to also engineer orthogonal LAP sequences.

**Imaging via Stimulated Emission Depletion Microscopy and Electron Microscopy with Resorufin Ligase.** Owing to the ∼250-nm diffraction barrier of visible light, small or densely packed cellular structures and complexes can only be resolved using superresolution microscopic approaches. We tested whether resorufin ligase could be used in conjunction with superresolution fluorescence imaging by stimulated emission depletion (STED) (31). Living CV-1 cells expressing LAP-tagged vimentin were labeled with resorufin ligase and resorufin-$AM_2$. Imaging by STED gave superior differentiation between individual vimentin filament bundles (∼80-nm resolution) compared with conventional confocal microscopy (Fig. 4*A*).

Electron microscopy (EM) is another powerful approach to study cellular samples at very high spatial resolution. We explored the ability of resorufin ligase to generate contrast for EM. Certain fluorophores in the excited state are known to photooxidize diaminobenzidine (DAB) into a locally deposited polymer (scheme in Fig. 4*B*) (13, 14, 32). This polymer in turn recruits osmium, which is electron-dense and gives EM contrast. We labeled vimentin in COS-7 cells using the LAP-F peptide, which increased photooxidation efficiency compared with LAP (*SI Appendix*, Fig. S9*C*). After osmium staining we observed dense deposits by brightfield imaging (Fig. 4*B*). EM imaging then revealed the localization of single ∼10-nm-wide vimentin filaments (Fig. 4*C*). Previous EM of intermediate filaments relied on extensive detergent extraction to remove confounding features such as microfilaments and microtubules (33) or used immunogold staining, which also must be preceded by detergent solubilization of membranes to allow antibody access (34). In contrast, the detergent-free protocol used here preserves cellular ultrastructure, membranes, and organelles and allowed us to visualize the relationship between vimentin intermediate filaments and endogenous cellular features. For example, Fig. 4*C* shows filaments bordering the cell nucleus and two individual filaments making apparent contact with a nuclear pore complex. A role for intermediate filaments in coordinating mechanical signals with nuclear activities such as transcription has previously been suggested (35, 36). In another example, we observed a close juxtaposition of mitochondria to filaments, especially for mitochondria in the periphery of the nucleus (Fig. 4*C*). Direct binding between vimentin and mitochondria has been suggested (37) and may play a role in mitochondrial trapping in cellular regions with high energy demand. Our resorufin ligase methodology provides a tool to examine the spatial and structural nature of these relationships.

## Discussion

In summary, we have used the enzyme redesign capabilities of Rosetta computation to create a new technology for protein labeling and imaging in living cells. PRIME with resorufin ligase can be used to study specific cellular proteins in an optimal spectral window while minimizing steric perturbation to that protein. Thus, PRIME can be an attractive alternative to red fluorescent proteins such as mCherry, which is 15 times larger, in cases where bulky tags are not tolerated [such as for β-actin shown in this work and neuroligin-1 shown elsewhere (38, 39)]. Our study shows that despite the posttranslational nature of our labeling the tagging specificity is exceptionally specific, comparable to that obtained by direct genetic fusion to fluorescent proteins.

Apart from conventional fluorescence microscopy, we showed that resorufin PRIME can also be used for superresolution fluorescence imaging by STED and for EM via photooxidation of DAB. Such multimodality tags are rare but provide great versatility for biological applications. However, the cost of tag versatility is that resorufin's photophysical properties are not highly optimal for either long-term fluorescence imaging or for highly efficient photooxidation. For example, miniSOG has a 12- to 20-fold higher quantum yield for $^1O_2$ generation (14, 40), and Cy3 is 30 times more photostable than resorufin (41).

From the standpoint of computational design, our work is notable in several respects. First, the redesign from lipoic acid recognition to resorufin recognition required a larger change in size, shape, and location of the binding pocket than in previous enzyme substrate specificity redesigns and began with a wild-type template that had no detectable activity for resorufin ligation. Despite this, our design lost less than $10^2$-fold catalytic efficiency compared wild-type activity, whereas a previous redesign of guanine deaminase lost ∼$10^7$-fold catalytic efficiency (18). This enabled

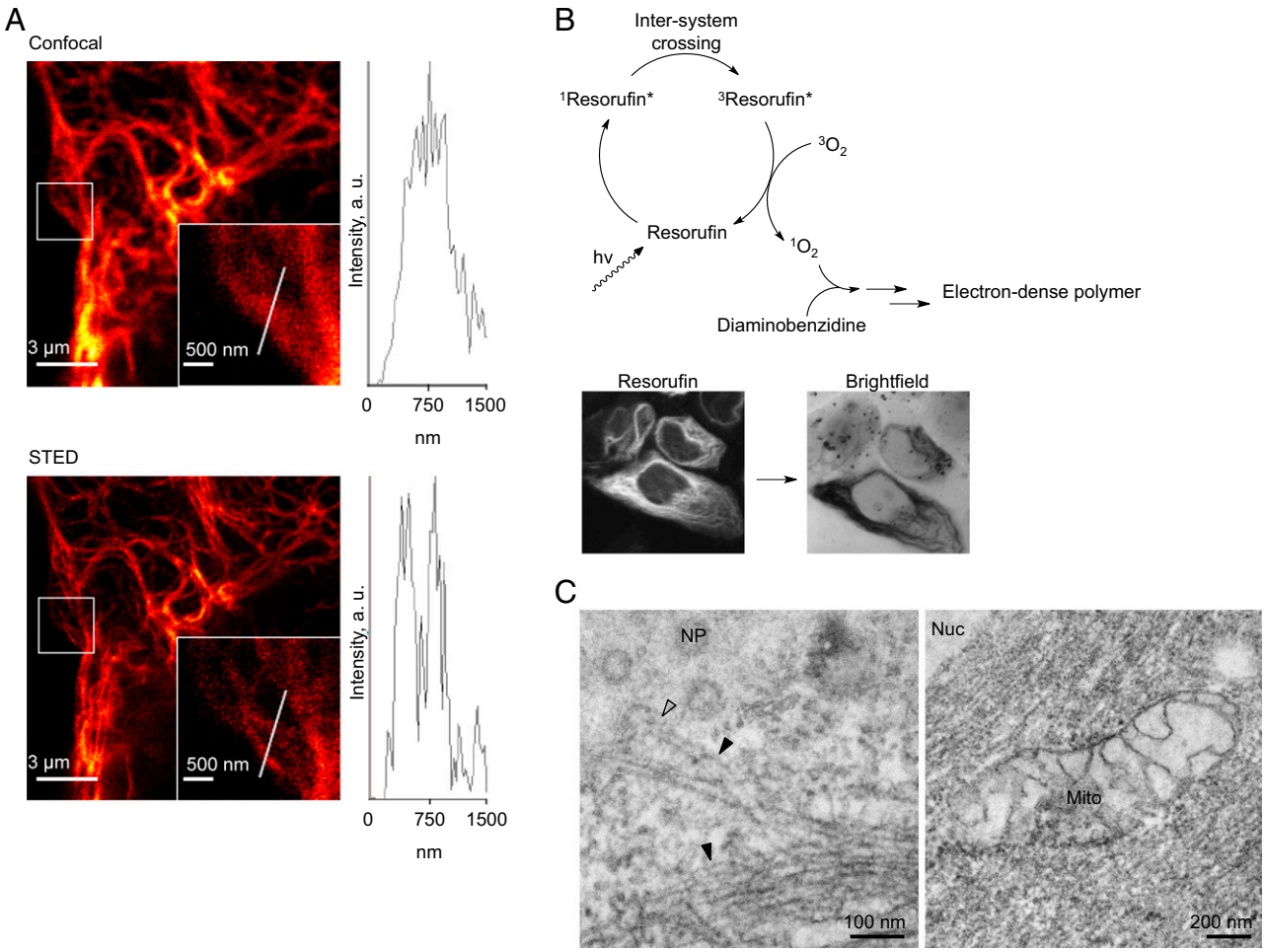


**Fig. 4.** Superresolution cellular protein imaging with resorufin ligase. (*A*) Live-cell imaging of resorufin-labeled vimentin intermediate filaments in CV-1 cells by confocal microscopy (*Upper*) and STED microcroscopy (*Lower*). Cross-sectional analysis of vimentin fluorescence is shown at the right. STED (resolution ~80 nm) was able to resolve filaments ~350 nm apart, whereas confocal (resolution ~300 nm) could not. (*B*) (*Upper*) Scheme for resorufin-catalyzed photooxidation of diaminobenzidine for EM. Resorufin in the excited singlet state ($^1$Resorufin*) undergoes intersystem crossing into the triplet state, which then generates singlet oxygen ($^1O_2$). Singlet oxygen polymerizes diaminobenzidine; subsequent staining by $OsO_4$ generates an electron-dense polymer for EM. (*Lower*) Osmium-stained polymers on vimentin intermediate filaments visualized at low magnification under brightfield imaging correlates with resorufin fluorescence. (*C*) (*Left*) Vimentin filaments (solid arrowheads) were observed to contact nuclear pores (hollow arrowhead). (*Right*) Juxtanuclear mitochondria were observed to be encased by and associated with vimentin filament bundles. Mito, mitochondrion; NP, nuclear pore; Nuc, nucleus.

our designed ligase to have practical utility without the need for further directed evolution of catalytic efficiency. Second, although ~$10^9$ LplA variants were explored in silico, there was an unusually strong convergence toward a single sequence, and the top-ranked conformer of this sequence closely resembled the actual crystal structure. Our work illustrates the power of computational design to develop enzymes with practical utility for cell biology.

## Materials and Methods

**Protein Purification for in Vitro Enzymatic Reactions and Cell-Surface Resorufin Labeling.** LplA mutants with an N-terminal $His_6$ tag and E2p lipoyl domain were purified as previously reported (42). LplA was dialyzed against and stored in 20 mM Tris·HCl, pH 7.5, containing 10% (vol/vol) glycerol and 1 mM DTT, at –80 °C. E2p protein was dialyzed against 20 mM PBS, pH 7.4, and stored at –80 °C. Protein concentrations were determined by the bicinchoninic acid assay (Thermo Scientific).

**HPLC Assay of Enzyme Activity.** Resorufin ligation reactions are typically assembled with 0.5–2 μM enzyme, 200 μM LAP (GFEIDKVWYDLDA), 10–500 μM resorufin, 2 mM ATP, and 5 mM $Mg(OAc)_2$ in Dulbecco's PBS, pH 7.4, containing 10% (vol/vol) glycerol. Reactions were carried out at 30 °C and quenched by addition of ethylenediaminetetracetic acid at 50 mM final concentration. Reaction mixtures were analyzed by one of two HPLC systems. In system 1, 50 μL of the quenched mixture was resolved by reverse-phase HPLC (Varian Prostar) using a $C_{18}$ column (Microsorb-MV 300–5) under a 25–60% (vol/vol) acetonitrile linear gradient over 20 min. Both $H_2O$ and acetonitrile solvents were supplemented with 0.1% trifluoroacetic acid acid. In system 2,10 μL of the quenched mixture was resolved by reverse-phase HPLC (Shimadzu UFLC XR) using a $C_{18}$ column (Supelco Ascentis Express ES-C18) under a 25–45% (vol/vol) acetonitrile linear gradient over 10 min. Both $H_2O$ and acetonitrile solvents were supplemented with 0.1% formic acid. Peptide and resorufin-peptide adducts were quantified by integrating their UV absorption peaks at 210 nm, with correction from resorufin absorption using a previously reported method (42). LAP and LAP-F peptides were synthesized and purified to >95% purity by GenScript.

**Cloning and Mutagenesis.** LplA mutants for bacterial expression and purification were generated by QuikChange mutagenesis using a standard protocol (Stratagene). $^{E20A/F147A/H149G}$LplA (resorufin ligase) was generated by two sequential QuikChange steps (E→A, followed by F→A and H→G) from the wild-type sequence and was inserted into mammalian expression plasmids using standard restriction digestion and ligation protocols.

**Mammalian Cell-Line Culture and Transfection.** Unless otherwise stated, human embryonic kidney 293T (HEK), HeLa, and COS-7 cells (all from American Type Culture Collection) were cultured as a monolayer on 150-μm-thick glass coverslips

in complete growth medium: MEM (Mediatech) supplemented with 10% (vol/vol) FBS (PAA Laboratories) at 37 °C and under 5% (vol/vol) $CO_2$. For HEK cells, coverslips were pretreated with 50 μg/mL human fibronectin (Millipore). Cells were typically transfected with 200–400 ng plasmid DNA per 1 $cm^2$ at ∼70% confluence using Lipofectamine 2000 (Life Technologies) according to the manufacturer's instructions then labeled 16–24 h after transfection.

**Dissociated Rat Neuron Culture and Transfection.** All animals were housed and cared for, and experiments were conducted, in accordance with the Massachusetts Institute of Technology Committee on Animal Care guidelines (assurance no. A-3125-01) as specifically approved as part of animal protocol no. 0910-076-13. Sprague–Dawley rat pups were euthanized at embryonic day 18. Cortical tissue was digested with papain (Worthington) and DNaseI (Roche), then plated in MEM + L-glutamine (Sigma) supplemented with 10% (vol/vol) FBS (PAA Laboratories) and B27 (Life Technologies) on glass coverslips pretreated wih poly-D-lysine (Sigma) and mouse laminin (Life Technologies). At 3 d in vitro, half of the growth medium was replaced with Neurobasal (Life Technologies) supplemented with B27 and GlutaMAX (Life Technologies). Neuron transfection was performed at 5 d in vitro, using half the amount of Lipofectamine 2000 recommended by the manufacturer. Cells were labeled and imaged at 9 d in vitro.

**General Protocol for Resorufin Labeling Inside Cells.** HEK, HeLa, and COS-7 cells on glass coverslips were rinsed twice with serum-free MEM then treated with MEM containing 5 μM resorufin **2**-$AM_2$ for 10–30 min at 37 °C. The cells were then rinsed three times with complete growth medium and left at 37 °C for 40 min to 1 h for excess dye to wash out of cells then imaged live in Dulbecco's PBS (DPBS), pH 7.4. During dye washout the medium was replaced with fresh complete growth medium at 10 and 20 min after initial rinsing to improve washout efficiency.

Dissociated rat neurons on glass coverslips were labeled in the same way except that they were treated with 2.5 μM resorufin **2**-$AM_2$ for 30 min and dye washout required 2 h in Neurobasal supplemented with GlutaMAX and B27. Cells were imaged live in Tyrode's buffer (145 mM NaCl, 1.25 mM $CaCl_2$, 3 mM KCl, 1.25 mM $MgCl_2$, 0.5 mM $NaH_2PO_4$, and 10 mM glucose in 10 mM Hepes, pH 7.4).

**Live-Cell Fluorescence Microscopy.** HEK, HeLa, and COS-7 cells placed in DPBS or rat neurons in Tyrode's buffer were imaged using a Zeiss AxioObserver.Z1 inverted confocal microscope with a 40× or 63× oil-immersion objective. The spinning disk confocal head was manufactured by Yokogawa. The following laser excitation sources and filter sets were used: BFP and coumarin (405 excitation, 438/30 emission, 450 dichroic); YFP and GFP (491 excitation, 535/30 emission, 502 dichroic); resorufin, mApple, and TMR (561 excitation, 605/20 emission, 585 dichroic); and Alexa Fluor 647 (647 excitation, 680/30 emission, 660 dichroic). Resorufin imaging at 561 nm was typically performed at ∼50 mW/$cm^2$ irradiance. Acquisition times ranged from 100 to 1,000 ms. Images were acquired and processed using SlideBook software version 5.0 (Intelligent Imaging Innovations).

**Purification of Resorufin Ligase for Crystallization Experiments (Fig. 2*C* and *SI Appendix*, Fig. S4 and Table S1).** Resorufin ligase with an N-terminal $His_6$ tag followed by a Tobacco Etch Virus (TEV) protease cleavage sequence was expressed in *E. coli* and purified by immobilized metal affinity chromatography as described in *Materials and Methods*. Purified protein was dialyzed against LplA buffer [20 mM Tris·HCl (pH 7.5), 10% (vol/vol) glycerol, and 1 mM DTT] then dialyzed against TEV protease cleavage buffer [50 mM Tris·HCl (pH 8.0), 0.5 mM EDTA, and 1 mM DTT] and subsequently treated with AcTEV protease (Life Technologies) at 4 °C for 48 h in the same buffer to remove the $His_6$ tag. The cleaved tag and AcTEV protease (also contains $His_6$ tag) were removed by immobilized metal affinity chromatography. The flow-through containing tag-less resorufin ligase was dialyzed against LplA buffer and further purified by size-exclusion chromatography on a Superdex 75 HiLoad 26/600 column (GE Healthcare) developed in LplA buffer at 4 °C, using the ÄKTA purifier system (GE Healthcare). Elution was monitored at 250 nm absorbance and the pure fractions were pooled, then concentrated to ∼8 mg/mL using Amicon ultracentrifugal filter units, 10-kDa molecular weight cutoff (Sigma-Aldrich).

**Determination of the Crystal Structure of Resorufn Sulfamoyladenosine-Bound Resorufin Ligase (Fig. 2*C* and *SI Appendix*, Fig. S4 and Table S1).** Crystallization of the sulfamoyladenosine analog bound structure was carried out in a hanging drop vapor diffusion setup, using 2 μL of 5.6 mg/mL resorufin ligase containing 1 mM resorufin sulfamoyladenosine, 1 mM $Mg(OAc)_2$, and 1 mM DTT mixed with 2 μL of precipitant solution [11% (wt/vol) PEG 20,000 and 0.15 M MES:NaOH, pH 6.5]. Drops were incubated at 4 °C in the dark, and red-colored crystalline plates appeared after ∼5 d. Crystals were looped and washed through a cryoprotection solution of 80% (vol/vol) precipitant solution [12% (wt/vol) PEG 20,000 and 0.2 M MES:NaOH, pH 6.5] and 20% (vol/vol) glycerol. Crystals were then cryocooled by direct submersion into liquid nitrogen.

Diffraction data were collected at the Advanced Photon Source and processed using HKL-2000 (43). Owing to significant anisotropy in the a* axis of the dataset [determined by the Diffraction Anisotropy Server (44)], blind regions were included at the top and bottom of each frame during integration to avoid merging absent reflections into the dataset. Although resulting data have lower redundancy and lower completeness in the high-resolution shell compared with the apo data (*SI Appendix*, Table S1), data quality was sufficient to solve the structure and evaluate ligand binding.

The ligand-bound structure was solved by molecular replacement in Phaser (45) using a model of lipoyl-AMP–bound LplA with waters and ligands removed [PDB ID code 3A7R (16), Z-score 28.1, 4.5 Å high resolution cutoff]. Four molecules of the ligase were found in the asymmetric unit. Model building, refinement, and structural validation were carried out as described in *SI Appendix* for the "apo" structure, with the exception that non-crystallographic symmetry (NCS) restraints were used in refinement owing to the lower resolution. In particular, each of the four monomers in the asymmetric unit was used as a group for torsion NCS weighting. Statistics for the final structure are shown in *SI Appendix*, Table S1.

**Live-Cell Resorufin Labeling and Imaging of Proteins in Various Cell Lines (Fig. 3 *A*, *C*, and *D*).** Cells were transfected with indicated constructs and labeled and imaged live as described in *Materials and Methods*. Labeling and dye washout times for HEK cells were 10 min and 45 min, respectively. Labeling and dye washout times for HeLa and COS-7 cells were 20 min and 1 h, respectively.

**Analysis of Resorufin Labeling Specificity by SDS/PAGE (Fig. 3*B*).** HEK cells grown in a six-well plate (9.5 $cm^2$ per well) were transfected and labeled with resorufin **2**-$AM_2$ as in Fig. 3*A* (plasmid quantity scaled up proportionally) then lifted by gentle trituration and lysed by three freeze–thaw cycles in hypotonic lysis buffer (5 mM $MgCl_2$ and 1 mM Hepes, pH 7.5) containing 1× protease inhibitor mixture (Sigma) and 500 μM phenylmethanesulfonylfluoride. The lysate was clarified by centrifugation at 8,000 × *g* for 10 min at 4 °C. The supernatant was then boiled in the presence of SDS and resolved on an 8% (wt/vol) SDS polyacrylamide gel. Resorufin fluorescence was imaged on a Fujifilm FLA-9000 image scanner with 532-nm excitation and a green long-pass filter. The same gel was then stained by Coomassie and reimaged under white light.

**Comparison of β-Actin Localization with LAP, mApple, or HaloTag (Fig. 3*D*).** HeLa cells were transfected with H2B-YFP (a nucleus marker) and one of the following: (*i*) resorufin ligase + LAP–β-actin, (*ii*) mApple–β-actin, or (*iii*) HaloTag–β-actin. Eighteen hours after transfection, the LAP–β-actin cells were labeled as in Fig. 3*C* then imaged live; mApple–β-actin cells were imaged without further treatment. HaloTag–β-actin cells were labeled with 5 μM tetramethylrhodamine ligand (Promega) for 15 min then imaged live after a 30-min washout of excess ligand.

**Resorufin Labeling of Vimentin Intermediate Filaments for Live-Cell STED Imaging (Fig. 4*A*).** CV-1 cells, grown on 18-mm coverslips in 24-well plates, were cotransfected with GFP-tagged resorufin ligase and C-myc–tagged vimentin-LAP. The next day, cells were incubated with 10 μM resorufin **2**-$AM_2$ for 10 min, followed by a single rinse and further 60-min incubation in complete growth medium. Before imaging, cells were washed twice with Opti-MEM medium (Invitrogen) supplemented with 2 mg/mL glucose. Coverslips were transferred to custom-made holders, overlaid with ∼500 mL of Opti-MEM, and imaged at room temperature. The STED setup used has been described previously (46). Excitation and STED beams were derived from a single supercontinuum laser source with 570-nm and 720-nm light used for excitation and stimulated depletion of resorufin, respectively. The fluorescence signal was separated by appropriate filters and detected in the spectral range of 580–620 nm. Representative confocal images were obtained by imaging the sample in the absence of the STED beam.

**Resorufin Labeling of Vimentin Followed by Photooxidation of Diaminobenzidine for EM (Fig. 4 *B* and *C*).** COS-7 cells expressing vimentin-LAP and resorufin ligase grown on poly-D-lysine–coated glass-bottom culture dishes (MatTek) were labeled with resorufin **2**-$AM_2$ as in Fig. 3*C*. After dye and colcemid washout, cells were fixed in 2% (wt/vol) glutaraldehyde (Electron Microscopy Sciences) in cacodylate buffer (100 mM, pH 7.4) at 4 °C for ∼24 h then rinsed in the same

buffer three times on ice. Cells were subsequently treated with 50 mM glycine to quench unreacted aldehydes, followed by 10 mM potassium cyanide and 5 mM aminotriazole in the cacodylate buffer for 20 min on ice to suppress background. Photooxidation was performed using a Leica SPI II inverted confocal microscope equipped with a 150-W xenon light source. Labeled cells were located by epifluorescence and treated with a fresh solution of diaminobenzidine (prepared by dissolving 5.4 mg diaminobenzidine in 1 mL 0.1 N HCl and diluting to 10 mL total volume using cacodylate buffer; Sigma). A stream of oxygen gas was blown over the surface of the solution and the cells were illuminated using a 562/40 filter (Semrock) at full intensity for 10–20 min until a brown reaction product appeared. These illumination conditions are much more intense than for live-cell imaging, such that most fluorescence was photobleached after the 10- to 20-min treatment. The cells were then rinsed in cold cacodylate buffer and postfixed with 1% osmium tetroxide on ice. After rinses in cold water, cells were either stained with 2% (wt/vol) aqueous uranyl acetate at 4 °C overnight *en bloc* or directly dehydrated in cold ethanol series [20, 50, 70, 90, and 100% (vol/vol)] for 3 min each on ice, followed by a room temperature rinse in 100% ethanol. Cells were embedded in Durcupan ACM resin (Electron Microscopy Sciences). Standard 80-nm-thick sections were imaged using a JEOL 1200 EX transmission electron microscope operated at 80 kV. Cells in Fig. 4*B* were treated with 1 μg/mL colcemid (Sigma) for 4 h before addition of resorufin-$AM_2$.

**ACKNOWLEDGMENTS.** Birka Hein [Max Planck Institute (MPI) for Biophysical Chemistry] performed preliminary STED imaging experiments. Stefan Hell (MPI for Biophysical Chemistry) provided experimental advice and performed critical reading of the manuscript. Chayasith Uttamapinant [Massachusetts Institute of Technology (MIT)] provided the coumarin compounds and the LAP–β-actin, vimentin-LAP, LAP-MAP2, and HaloTag–β-actin plasmids. Carolyn Kwa (MIT) and Ken Loh (MIT) provided assistance with neuron cultures. Justin Cohen (MIT) and Samuel Thompson (MIT) provided LplA protein. Katharine White (MIT) provided the LAP-CaaX, LAP-NLS, and LAP-NES plasmids. Michael Davidson (Florida State University) provided the mApple–β-actin plasmid. We thank Kyle Gee (Life Technologies) for helpful discussions about the resorufin fluorophore. Diffraction data were obtained at the Advanced Photon Source on the Northeastern Collaborative Access Team beamlines, which are supported by Award RR-15301 from the National Center for Research Resources at the National Institutes of Health (NIH). Use of the Advanced Photon Source, an Office of Science User Facility operated for the US Department of Energy (DOE) Office of Science by Argonne National Laboratory, was supported by the US DOE under Contract DE-AC02-06CH11357. This work was funded by NIH Grants DP1 OD003961 and R01 GM072670 (to A.Y.T.), NIH Grant GM103412 (to M.H.E.), and the American Chemical Society (A.Y.T.). C.L.D. is a Howard Hughes Medical Institute (HHMI) Investigator. L.G.N. acknowledges support from a National Science Foundation Minority Post-Doctoral Fellowship. A.Z.Y. acknowledges support from the Lord Foundation and the HHMI-Massachusetts Institute of Technology Summer Research Program in Chemical Biology.

1. Moritz OL, Tam BM, Papermaster DS, Nakayama T (2001) A functional rhodopsin-green fluorescent protein fusion protein localizes correctly in transgenic Xenopus laevis retinal rods and is expressed in a time-dependent pattern. *J Biol Chem* 276(30):28242–28251.
2. Marsh DR, Holmes KD, Dekaban GA, Weaver LC (2001) Distribution of an NMDA receptor:GFP fusion protein in sensory neurons is altered by a C-terminal construct. *J Neurochem* 77(1):23–33.
3. van de Linde S, et al. (2013) Investigating cellular structures at the nanoscale with organic fluorophores. *Chem Biol* 20(1):8–18.
4. Müller T, Schumann C, Kraegeloh A (2012) STED microscopy and its applications: New insights into cellular processes on the nanoscale. *ChemPhysChem* 13(8):1986–2000.
5. Los GV, et al. (2008) HaloTag: A novel protein labeling technology for cell imaging and protein analysis. *ACS Chem Biol* 3(6):373–382.
6. Keppler A, et al. (2003) A general method for the covalent labeling of fusion proteins with small molecules in vivo. *Nat Biotechnol* 21(1):86–89.
7. Jing C, Cornish VW (2013) A fluorogenic TMP-tag for high signal-to-background intracellular live cell imaging. *ACS Chem Biol* 8(8):1704–1712.
8. Stroffekova K, Proenza C, Beam KG (2001) The protein-labeling reagent FLASH-EDT2 binds not only to CCXXCC motifs but also non-specifically to endogenous cysteine-rich proteins. *Pflugers Arch* 442(6):859–866.
9. Lang K, et al. (2012) Genetic encoding of bicyclononynes and trans-cyclooctenes for site-specific protein labeling in vitro and in live mammalian cells via rapid fluorogenic Diels-Alder reactions. *J Am Chem Soc* 134(25):10317–10320.
10. Uttamapinant C, et al. (2010) A fluorophore ligase for site-specific protein labeling inside living cells. *Proc Natl Acad Sci USA* 107(24):10914–10919.
11. Xu W, Kong JS, Yeh Y-TE, Chen P (2008) Single-molecule nanocatalysis reveals heterogeneous reaction pathways and catalytic dynamics. *Nat Mater* 7(12):992–996.
12. Tour O, Meijer RM, Zacharias DA, Adams SR, Tsien RY (2003) Genetically targeted chromophore-assisted light inactivation. *Nat Biotechnol* 21(12):1505–1508.
13. Gaietta G, et al. (2002) Multicolor and electron microscopic imaging of connexin trafficking. *Science* 296(5567):503–507.
14. Shu X, et al. (2011) A genetically encoded tag for correlated light and electron microscopy of intact cells, tissues, and organisms. *PLoS Biol* 9(4):e1001041.
15. Cohen JD, Thompson S, Ting AY (2011) Structure-guided engineering of a Pacific Blue fluorophore ligase for specific protein imaging in living cells. *Biochemistry* 50(38):8221–8225.
16. Fujiwara K, et al. (2010) Global conformational change associated with the two-step reaction catalyzed by Escherichia coli lipoate-protein ligase A. *J Biol Chem* 285(13):9971–9980.
17. Richter F, Leaver-Fay A, Khare SD, Bjelic S, Baker D (2011) De novo enzyme design using Rosetta3. *PLoS ONE* 6(5):e19230.
18. Murphy PM, Bolduc JM, Gallaher JL, Stoddard BL, Baker D (2009) Alteration of enzyme specificity by computational loop remodeling and design. *Proc Natl Acad Sci USA* 106(23):9215–9220.
19. Ashworth J, et al. (2006) Computational redesign of endonuclease DNA binding and cleavage specificity. *Nature* 441(7093):656–659.
20. Chen C-Y, Georgiev I, Anderson AC, Donald BR (2009) Computational structure-based redesign of enzyme activity. *Proc Natl Acad Sci USA* 106(10):3764–3769.
21. Puthenveetil S, Liu DS, White KA, Thompson S, Ting AY (2009) Yeast display evolution of a kinetically efficient 13-amino acid substrate for lipoic acid ligase. *J Am Chem Soc* 131(45):16430–16438.
22. Fujiwara K, et al. (2005) Crystal structure of lipoate-protein ligase A from Escherichia coli. Determination of the lipoic acid-binding site. *J Biol Chem* 280(39):33645–33651.
23. Van de Vijver P, et al. (2009) Synthetic microcin C analogs targeting different aminoacyl-tRNA synthetases. *J Bacteriol* 191(20):6273–6280.
24. Brown PH, Cronan JE, Grøtli M, Beckett D (2004) The biotin repressor: Modulation of allostery by corepressor analogs. *J Mol Biol* 337(4):857–869.
25. Reche PA (2000) Lipoylating and biotinylating enzymes contain a homologous catalytic module. *Protein Sci* 9(10):1922–1929.
26. Green DE, Morris TW, Green J, Cronan JE, Jr, Guest JR (1995) Purification and properties of the lipoate protein ligase of Escherichia coli. *Biochem J* 309(Pt 3):853–862.
27. Lavis LD, Chao T-Y, Raines RT (2011) Synthesis and utility of fluorogenic acetoxymethyl ethers. *Chem Sci* 2(3):521–530.
28. Riedl J, et al. (2008) Lifeact: a versatile marker to visualize F-actin. *Nat Methods* 5(7):605–607.
29. Marmé N, Knemeyer J-P, Sauer M, Wolfrum J (2003) Inter- and intramolecular fluorescence quenching of organic dyes by tryptophan. *Bioconjug Chem* 14(6):1133–1139.
30. Adams SR, et al. (2002) New biarsenical ligands and tetracysteine motifs for protein labeling in vitro and in vivo: Synthesis and biological applications. *J Am Chem Soc* 124(21):6063–6076.
31. Hell SW (2007) Far-field optical nanoscopy. *Science* 316(5828):1153–1158.
32. Deerinck TJ, et al. (1994) Fluorescence photooxidation with eosin: A method for high resolution immunolocalization and in situ hybridization detection for light and electron microscopy. *J Cell Biol* 126(4):901–910.
33. Jones JCR, Goldman AE, Steinert PM, Yuspa S, Goldman RD (1982) Dynamic aspects of the supramolecular organization of intermediate filament networks in cultured epidermal cells. *Cell Motil* 2(3):197–213.
34. Katsumoto T, Mitsushima A, Kurimura T (1990) The role of the vimentin intermediate filaments in rat 3Y1 cells elucidated by immunoelectron microscopy and computergraphic reconstruction. *Biol Cell* 68(2):139–146.
35. Goldman R, et al. (1985) Intermediate filaments: Possible functions as cytoskeletal connecting links between the nucleus and the cell surface. *Ann N Y Acad Sci* 455:1–17.
36. Shimi T, Butin-Israeli V, Goldman RD (2012) The functions of the nuclear envelope in mediating the molecular crosstalk between the nucleus and the cytoplasm. *Curr Opin Cell Biol* 24(1):71–78.
37. Nekrasova OE, et al. (2011) Vimentin intermediate filaments modulate the motility of mitochondria. *Mol Biol Cell* 22(13):2282–2289.
38. Liu DS, Loh KH, Lam SS, White KA, Ting AY (2013) Imaging trans-cellular neurexin-neuroligin interactions by enzymatic probe ligation. *PLoS ONE* 8(2):e52823.
39. Liu DS, Phipps WS, Loh KH, Howarth M, Ting AY (2012) Quantum dot targeting with lipoic acid ligase and HaloTag for single-molecule imaging on living cells. *ACS Nano* 6(12):11080–11087.
40. Bueno C, et al. (2002) The excited-state interaction of resazurin and resorufin with amines in aqueous solutions. Photophysics and photochemical reactions. *Photochem Photobiol* 76(4):385–390.
41. Cao H, et al. (2007) A red cy3-based biarsenical fluorescent probe targeted to a complementary binding peptide. *J Am Chem Soc* 129(28):8672–8673.
42. Fernández-Suárez M, et al. (2007) Redirecting lipoic acid ligase for cell surface protein labeling with small-molecule probes. *Nat Biotechnol* 25(12):1483–1487.
43. Otwinowski Z, Minor W (1997) . Processing of X-ray diffraction data collected in oscillation mode. *Methods in Enzymology*, ed Carter CW, Jr (Academic, New York), Vol 276, pp 307–326.
44. Strong M, et al. (2006) Toward the structural genomics of complexes: Crystal structure of a PE/PPE protein complex from Mycobacterium tuberculosis. *Proc Natl Acad Sci USA* 103(21):8060–8065.
45. McCoy AJ, et al. (2007) *Phaser* crystallographic software. *J Appl Cryst* 40(Pt 4):658–674.
46. Bückers J, Wildanger D, Vicidomini G, Kastrup L, Hell SW (2011) Simultaneous multi-lifetime multi-color STED imaging for colocalization analyses. *Opt Express* 19(4):3130–3143.
47. Ho BK, Gruswitz F (2008) HOLLOW: generating accurate representations of channel and interior surfaces in molecular structures. *BMC Struct Biol* 8:49.